Materials Today Bio 24 (2024) 100942

Contents lists available at ScienceDirect

Materials Today Bio

journal homepage: www.journals.elsevier.com/materials-today-bio

Multi-needle blow-spinning technique for fabricating collagen nanofibrous nerve guidance conduit with scalable productivity and high performance

Chun-Yi Yang [a,1], Zhaohui Hou [a,1], Peilun Hu [a,b], Chengli Li [a,b], Zifan Li [a], Zekun Cheng [a], Shuhui Yang [c], Pengchao Ma [a], Zhe Meng [a], Hui Wu [a], Yongwei Pan [b], Zheng Cao [a,d], Xiumei Wang [a,*]

[a] State Key Laboratory of New Ceramics and Fine Processing, Key Laboratory of Advanced Materials of Ministry of Education, School of Materials Science and Engineering, Tsinghua University, Beijing, 100084, PR China
[b] Department of Orthopaedics Beijing Tsinghua Changgung Hospital, School of Clinical Medicine, Tsinghua University, Beijing, 102218, PR China
[c] School of Materials Science and Engineering, Zhejiang-Mauritius Joint Research Center for Biomaterials and Tissue Engineering, Zhejiang Sci-Tech University, Hangzhou, 310018, PR China
[d] Center for Biomaterials and Regenerative Medicine, Wuzhen Laboratory, Tongxiang, 314500, PR China

ARTICLE INFO

Keywords:
Blow spinning technique
Nerve guidance conduit
Collagen nanofibers
Peripheral nerve regeneration
Scalable productivity

ABSTRACT

Nerve guidance conduits (NGCs) have been widely accepted as a promising strategy for peripheral nerve regeneration. Fabricating ideal NGCs with good biocompatibility, biodegradability, permeability, appropriate mechanical properties (space maintenance, suturing performance, etc.), and oriented topographic cues is still current research focus. From the perspective of translation, the technique stability and scalability are also an important consideration for industrial production. Recently, blow-spinning technique shows great potentials in nanofibrous scaffolds fabrication, possessing high quality, high fiber production rates, low cost, ease of maintenance, and high reliability. In this study, we proposed for the first time the preparation of a novel NGC via blow-spinning technique to obtain optimized performances and high productivity. A new collagen nanofibrous neuro-tube with the bilayered design was developed, incorporating inner oriented and outer random topographical cues. The bilayer structure enhances the mechanical properties of the conduit in dry and wet, displaying good radial support and suturing performance. The porous nature of the blow-spun collagen membrane enables good nutrient delivery and metabolism. The *in vitro* and *in vivo* evaluations indicated the bilayer-structure conduit could promoted Schwann cells growth, neurotrophic factors secretion, and axonal regeneration and motor functional recovery in rat.

1. Introduction

Peripheral nerve injury (PNI) caused by trauma, diseases, or congenital defects often leads to serious sensory and/or motor dysfunctions, affecting millions of patients worldwide each year. Unlike central nervous system (CNS) injury that typically results in permanent neurological disability, peripheral nerve system (PNS) shows great potential for self-repair through the regrowth of damaged axons [1]. Therefore, diverse grafts including autograft, allograft, and synthetic constructs have been successfully developed for promoting PNI repair with defect exceeding critical size. Nevertheless, the clinical outcomes are still far from satisfactory. Autologous nerve transplantation is commonly considered as the gold standard for treating large-gap PNI in clinical practice because of its advantages of high biocompatibility, appropriate extracellular matrix, and axon-oriented structure [2,3]. However, the drawbacks such as limited donor availability, donor site damage, size and mismatch, nerve tumor formation, secondary incisions, and poor functional recovery cannot be ignored, which often restrict its applications in clinic. Therefore, nerve guidance conduits (NGCs) have been extensively researched as a substitute for autologous nerve transplantation. They function as tubular bridges to connect the proximal and distal stumps of the injured nerve to provide a confined environment for assisting in the growth of the proximal nerve towards the distal end. Additionally, NGCs can act as protective barriers,

* Corresponding author.
E-mail address: wxm@mail.tsinghua.edu.cn (X. Wang).
[1] These authors contributed equally to this work.

https://doi.org/10.1016/j.mtbio.2024.100942
Received 11 October 2023; Received in revised form 18 December 2023; Accepted 2 January 2024
Available online 4 January 2024

providing a buffer zone to the injured area and preventing secondary injury [4].

To achieve the good performances surpassing the autografts, many design strategies for NGCs focusing biomaterials, fabrication techniques, and surface and intraluminal microenvironment modifications have been extensively investigated [5]. However, there is still a lack of an ideal NGC in clinical practice currently. For obtaining ideal NGCs, development of the hollow tubes with good biocompatibility, biodegradability, permeability, appropriate mechanical properties (space maintenance, suturing performance, etc.), and oriented topographic cues is a prerequisite [6]. Conventional techniques for fabricating hollow NGCs include injection molding, melting extrusion, braiding, and solvent casting/freeze-drying [7]. These NGCs cannot possess good combination of appropriate mechanical properties, permeability, and biomimetic nanoscale topography. Some advanced techniques, such as electrospinning and 3D printing have been widely explored in academic research [8,9]. Electrospinning is the most commonly used technique for fabricating nanofibrous textiles that can mimic the nanofiber structure of natural ECM, which could optimize the mechanical and biological properties for modulating cellular behaviors. Nevertheless, electrospinning process involves the load of an electric field to draw polymer solution or melt into nanofibers, which requires the solution and collector to be conductive, thus greatly limiting the biomaterial and solvent selection and its applications [10]. Consequently, it is difficult to prepare thick membrane or three-dimensional scaffolds using electrospinning because of the decreased conductivity with the deposition of the electrospun nanofibers. In addition, the fabrication efficiency of electrospinning is low for industrial scalable and cost-effective production.

In recent years, blow-spinning technique (BS) emerges as a novel technique to fabricate nanofibers in large batch. The main theoretical basis is the Bernoulli principle, which uses high-speed airflow instead of electric field as the driving force to spin ultrafine fibers from a solution [11,12]. Compared with electrospinning, the equipment for blow spinning is very simple, consisting of only a spray gun, compressed air source, and a polymer solution. Additionally, blow spinning does not require the use of high voltages or high temperature, which can simplify the production process and reduce the potential for environmental hazards. Another advantage of blow spinning is its ability to produce large quantities of nanofibers into different configuration of constructs at high production rates [13]. And our previous study indicated that the blow-spinning nanofibrous membrane had more fluffy and spongy structure than the electrospun one that contributed to the increased specific surface area and permeability for sufficient nutrition exchange, chemical-crosslinking, and cell adhesion and migration [14]. Therefore, we proposed for the first time the preparation of a novel NGC via blow spinning technique to obtain optimized performances including permeability, controllable biodegradability, radial mechanical support, suturing performance, and oriented nanofibrous guidance cue.

Unlike the single-needle blow spinning technique used previously, multi-needle blow-spinning technique was applied for the preparation of NGCs in this study. Considering the automated production process in industry, multi-needle blow-spinning is more suitable for stable production compared with the single-needle spray guns. Multi-needle blow spinning can further increase production efficiency for large-scale production due to its multi-needle layout [15]. Additionally, more uniform fiber distribution and network structure could be easily obtained using multi-needle blow-spinning. During the process of fiber collection in single-needle blow spinning, a dense center area and a sparse edge area are often observed due to the limitation of the air jet boundary range. This problem can be improved by adjusting the range of the air jet boundary and the arrangement of the needles.

Biomaterial selection is also crucial for optimal NGCs to exhibit favorable biocompatibility and biochemical signals for nerve regeneration. Currently, the commonly used biomaterials for NGCs include synthetic polymers (polycaprolactone (PCL), polylactide (PLA), poly(lactic-co-glycolic acid) (PLGA), polyvinylidene difluoride (PVDF)), natural macromolecule (collagen, chitosan, hyaluronic acid, silk fibroin), and a combination of both [5,16]. Compared with synthetic polymers, natural macromolecule materials have a superior biosafety, biocompatibility, and biodegradability, which makes them more suitable for the application as biological scaffolds [17]. Among them, collagen, as the most abundant structural protein in mammalian tissues, provides an important structural matrix for tissue development, maintenance, and regeneration, possessing excellent biocompatibility and low immunogenicity [18], which has led to collagen being the most FDA-certified material for NGCs [19]. Currently, there are many collagen-based NGCs in the market for PNI regeneration, such as NeuroGen®, NeuroFlex^{TM}, NeuroMatrix^{TM}, NeuroMend^{TM}, and NeuroWrap^{TM} [3,20]. Although these collagen conduits achieve good outcomes in clinic for the PNI cases with defects up to 20 mm, the drawbacks including poor mechanical properties, high swelling ratio, and fast degradation restrict the maintenance of the structural integrity of the conduits for long-distance defects repair. Therefore, an optimal fabrication method is very necessary for making porous collagen conduit with unique permeability, mechanical properties, and aligned surface nano-topography for better cell attachment and axonal regrowth longitudinally.

In this study, we developed a preparation process of collagen nanofibrous spongy membrane via multi-needle blow-spinning and rolled into a tube with a bilayer design, an outer layer of random fibers and an inner layer of oriented fibers. The inner aligned nanofiber alignment could provide topographical cues for modulating cellular behaviors and axonal regrowth. The outer interwoven nanofiber arrangement should be beneficial for the mechanical performances. The spongy feature of the collagen membrane and the rolling form of the tube could realize the controllable permeability and degree of chemical crosslinking. The *in vitro* biocompatibility and effect of topographical structure on Schwann cells were evaluated. And the bilayer structure of collagen nanofiber NGC was used for bridging 15-mm-long sciatic nerve defects in rats. The axonal regeneration and functional recovery were evaluated based on morphological, electrophysiological, and functional parameters.

2. Materials and methods

2.1. Fabrication of collagen membranes and tubes

The collagen membranes were fabricated according to previously reported [14]. Briefly, collagen solution was prepared by dissolving 4 g bovine-origin type I collagen (Collagen Biotechnology Co. Ltd, China) in 20 mL acetic acid (15 % (v/v)) (Macklin, China) under continuous stirring 12 h. During the blow-spinning process, collagen solution was extruded through a syringe needle at a rate of 5 mL/h. The roller collector speed (150, 1200 rpm) was used to collect the random and oriented nanofibers (Fig. 1).

For the electrospinning membrane, the 6 wt% collagen was prepared by dissolving in hexafluoroisopropanol (HFIP). During electrospinning, the collagen solution loaded into a 5 mL syringe, ejected at the speed of 0.09 mL/h under a voltage of 25 kV and collected by low-speed (150 rpm) collector to obtain random nanofibers.

The cylindrical rod with a diameter of 1.6 mm made of polytetrafluoroethylene is used to roll the random collagen membrane (long × wide × thick, 40 mm × 20 mm × 0.25 mm) into a tube shape. The tubes were soaked in the chemical crosslinking solution (50 mM N-ethyl-N ¢-(3-dimethylaminopropyl) carbodiimide hydrochloride (EDC; Sigma-Aldrich, St. Louis, MO) and 25 mM N-hydroxysulfosuccinimide sodium salt (NHS, Sigma-Aldrich, St. Louis, MO)) in 90 % ethanol for 24 h at room temperature, then the random collagen NGC was obtained after washing and drying.

For the bilayer tube, the oriented collagen membrane (long × wide × thick, 12 mm × 20 mm × 0.25 mm) was rolled into a tube first, and then roll the random collagen membrane (long × wide × thick, 28 mm

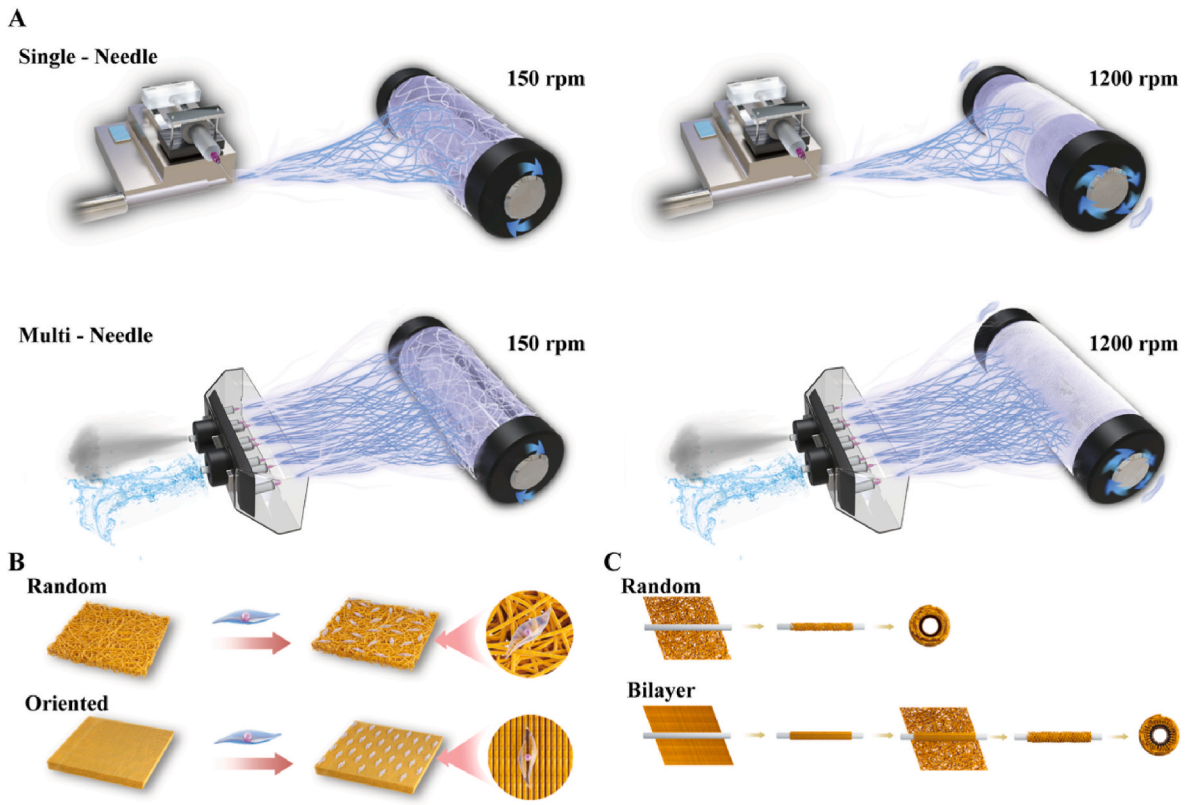

Fig. 1. Schematic diagram of preparing random and bilayer-structure nerve conduits through the blow spinning process. (A) Schematic diagram of blow spinning process. (B) Schematic illustration of the topographical effect of substrates on the alignment of cells. (C) Schematic flow chart of random nerve conduits and oriented nerve conduit structure along with key fabrication steps.

× 20 mm × 0.25 mm), forming a bilayer structure. The cross-linking method and steps are the same with those for random conduits.

After fabrication and before initiating animal studies, the conduits were securely stored in Eppendorf tubes and maintained in a desiccator.

The chitosan conduit was used as commercial product control. The fabrication of the chitosan conduits followed the guidelines outlined in a patent (Patent No. 01136314.2).

2.2. Characterization of collagen membrane

To examine the morphologies of collagen membrane, the samples were sputter-coated with a layer of Pt prior to a field-emission scanning electron microscope (FE-SEM, Zeiss, Germany). The distribution of fiber oriented in random membrane and aligned membrane were measured using Image J. The morphologies of the fibers were subsequently evaluated using a transmission electron microscope (TEM, G20, FEI Tecnai, China) operating at 200 kV.

For Fourier-transform infrared spectrometry (FTIR) analysis, the samples recorded using a FTIR spectrometer (TG-MS-FTIR-X70, NETZSCH Groups, Germany) with wavelength ranging from 4000 to 450 cm^{-1}.

The tensile strength of collagen NGC was measured using a universal mechanical testing machine (SHIMADZU AG-IC, Japan) with a 10 N load cell.

Water vapor transmission rates (WVTR) were measured according to ASTM E96 (American Society for Testing Materials)-standard test method. A centrifuge tube with 10 mL of DI water was covered with the collagen membrane at the top. The tube was placed into the chamber at 37 °C and 40 ± 2 % relative humidity. The weight of the assembly was recorded at regular intervals of every 2 h with the end point of 24 h and the slope was calculated [21].

$$WVTR = \frac{slope \times 24}{A} g \Big/ m^2 \bullet day \quad (1)$$

where A is the sample test area in m^2.

The degradation rate of the collagen membranes was examined after cross-linking. In brief, the collagen membranes (n = 6) for each group were dissolved in a solution of 0.1 mg/mL collagenase from Clostridium histolyticum Type I (≥125 CDU/mg, Sigma Aldrich, St. Louis, MO), which was further diluted in 2 mL distilled water. The dissolved membranes were then placed in an incubator and maintained at a constant temperature of 37 °C. The weight of the residual film was recorded at various time intervals until it completely disappeared.

The crosslinked collagen membranes (n = 3) were carefully dried using a critical point drying apparatus, and the weight of the membranes in their dried state was recorded. Subsequently, the collagen membranes were submerged in DI water for a period of 24 h until they reached a stable state. After removing them from the water, any excess surface moisture was gently wiped off, and the weight of the membranes in their wet state was recorded.

$$Swelling\ ratio = \frac{(Wet\ weight - Initial\ dry\ weight)}{(Initial\ dry\ weight) \times (Solvent\ density)} \quad (2)$$

The porosity is calculated with reference to the following formula, and the density of collagen is taken as 1.16 g/cm^3 [22].

$$Porosity = \left(1 - \frac{membrane\ density}{bulk\ material\ density}\right) \times 100 \quad (3)$$

The CD spectra of the collagen were measured using Chirascan plus (Applied Photophysics, UK). The collagen was dissolving to working concentrations of 0.1 g/mL in DI water and 200 μL of the samples were added to a quartz cuvette with a 1-mm path length. CD spectra were

recorded over the range of 180 nm–260 nm with a step size of 1 nm at room temperature. All samples were evaluated three times, and the data was averaged.

2.3. High-speed camera observation

To directly observe the BS process, a high-speed camera (Os7, Integrated Design Tools Inc., USA) with an F-mount lens (atx-i 100 mm F2.8 FF MACRO, Tokina, Japan) was utilized. To capture clear images with a short exposure time, a 100-W light-emitting diode lamp (LED-100-T, Visico, China) was used to continuously illuminate the spinning area. All high-speed images were captured at a frame rate of 8000 frames per second (fps), with a picture resolution of 1920 × 416 pixels and an exposure time of 60 μs. The obtained videos were analyzed using Motion Studio software. To view the high-speed videos, the images obtained at 8000 fps were played at a frame rate of 24 fps.

2.4. Cell morphology and gene expression of Schwann cells on membrane

Rat Schwann cells (RSCs) was obtained from the National Infrastructure of Cell Line Resource (RSC-96; 3111C0001CCC000664; Beijing, China) and cultured in Dulbecco's Modified Eagle Medium (DMEM) High Glucose complete medium (Procell Life Science & Technologies, Wuhan, China) in an incubator with 5 % CO_2 at 37 °C. RSCs were seeded on the surface of the collagen membranes at the density of 2×10^3 cells/well (96-well culture plate, n = 3). The fresh medium was changed every two days. At day 1, 3, and 5, cell proliferation was evaluated by cell counting kit-8 assay (CCK-8, DOJINDO, Japan) with 10 % working solution in cell culture medium for 2 h at 37 °C in incubator. The absorbance at 450 nm was measured using an EnSpire Multimode Plate Reader (PerkinElmer).

To visualize the cell morphology of RSCs on the membranes, the RSCs were seeded on the membrane at a density of 2×10^3 cells/well (96-well culture plate, n = 3) for three days. Then, the RSCs on the membrane were fixed with 4 % paraformaldehyde for 1 h and permeated with 0.3 % Triton X-100 solution for 10 min, followed by incubation in 10 % goat serum for 1 h at room temperature. Actin filaments and nuclei were stained with rhodamine-phalloidin (Cytoskeleton Inc., Denver, USA) and 4,6-diamidino-2-phenylindole (DAPI), respectively. The cells were imaged using a confocal laser scanning microscope (CLSM 980; Carl Zeiss, Germany). The cytoskeleton staining method of L929 is the same as that of RSCs.

To examine the cell function and gene expression, the RSCs were seeded on the membrane at a density of 1×10^4 cells/well (48-well culture plate, n = 3) for three days. Total mRNA was isolated using RNASimple Total RNA Kit (DP419, Tiangen, Beijing, China) and cDNA was reverse-transcribed by FastQuant RT Kit (KR-106, Tiangen, Beijing, China). Quantitative real-time polymerase chain reaction (qRT-PCR) was determined quantitatively on CFX96 Real-Time System (Bio-Rad Laboratories, Inc. China) using iTaq Universal SYBR Green Supermix (172–5122, Bio-Rad Laboratories, Inc. China). The sequences of primers used were listed in Table S1.

Lipopolysaccharide (LPS, Invitrogen)-activated RAW264.7 cells were utilized for *in vitro* assessment of the immunomodulatory function of oriented blow-spun collagen membranes. RAW264.7 cells were treated with 2 μg/mL LPS for 24 h to obtain LPS-activated cells. These cells were then seeded at a density of 5×10^4 cells/well (24-well culture plate, n = 3) onto electrospinning, random blow-spinning, and oriented blow-spinning collagen membranes for two days for use in PCR experiments. The RNA extraction procedure was consistent with that used for RSCs. For sterilization, the collagen membranes were soaked in 75 % alcohol for two days and exposed to ultraviolet light simultaneously. Before cell culture, 75 % alcohol was replaced with Phosphate buffered saline (PBS) and medium in a sterile environment.

2.5. Animal model of peripheral nerve injury

All procedures associated with animals were performed in accordance with the plan approved by Institutional Animal Care and Use Committee (IACUC) at Tsinghua University (Beijing, China). 24 SD rats (male, 300 g) were randomly divided into four experimental groups. To establish PNI models, SD rats were anesthetized by a single intraperitoneal injection of 2 % (w/v) pentobarbital sodium solution (2 mL/kg). The segment of sciatic nerve in the right lateral thigh was resected and removed to leave a 15-mm-long defect. For the Autograft group, the resected nerve segment was reversely re-implanted into the defect. For the Chitosan, Random and Bilayer group, both ends of the transected nerve were bridged with an empty tube (chitosan, random collagen or bilayer collagen tube). Spray bitters on the injured hind limbs every three days to prevent rats from licking and biting their toes. The collagen tubes sterilized by ^{60}Co irradiation and then used for animal experiment.

2.6. Electrophysiological assessment

At 12 weeks postoperatively, rats were deeply anesthetized, and electrophysiological examinations were performed on the sciatic nerves at the injured sides and normal side (n = 5). The nerve graft's proximal and distal ends were stimulated with electrical impulses, and the compound muscle action potentials (CMAPs) were measured on the gastrocnemius muscle. The groups were compared based on the latency and peak amplitude of the CMAPs.

2.7. Analysis of animal motor function

The CatWalk XT 10.6 gait analysis system (Noldus, Wageningen, The Netherlands) was used to assessed motor function recovery at 4, 8, and 12 weeks postoperatively (n = 5). Data were collected and analyzed, and sciatic function index (SFI) was calculated using a reported formula [23]:

$$SFI = 109.5\frac{(ETS - NTS)}{NTS} - 38.3\frac{(EPL - NPL)}{NPL} + 13.3\frac{(EIT - NIT)}{NIT} - 8.8 \quad (4)$$

where ETS is the operated experimental toe spread (the distance between the first and fifth toes), NTS is the normal toe spread, EPL is the operated experimental paw length, NPL is the normal paw length, EIT is the operated experimental intermediary toe spread (the distance between the second and fourth toes), and NIT is the normal inter-median toe spread.

2.8. Gastrocnemius muscle restoration

Twelve weeks after surgery, the wet weights gastrocnemius muscles from both side of SD rats were weighed immediately, and the ratio (injured/contralateral) was calculated (n = 5). The gastrocnemius muscles immersed in 4 % paraformaldehyde (PFA) at 4 °C for 7 days. They were embedded by paraffin wax and cut into 7 μm thick sections for Masson's trichrome staining. For each sample, 3 randomly selected fields were imaged and the muscle fibers were quantitatively analyzed with ImageJ.

2.9. Histology and morphometric analysis

For myelin observation, 12 weeks postoperatively, the operated side of sciatic nerves were retrieved, and nerve grafts were immersed in fixative solution (2.5 % glutaraldehyde + 2 % PFA) for 2 h, and in special osmium acid solution (1 % osmium tetroxide + 1.5 % Potassium hexacyanoferrate), dehydrated in series of graded ethanol solutions, embedded in Epon 812 epoxy resin, then the grafts were cut semithin sections and ultrathin sections (n = 3). The semithin sections were

stained with toluidine blue and observed using a light microscope (Pannoramic SCAN; 3DHistech, Hungary). The ultrathin sections were stained with 1 % uranyl acetate and observed under TEM (JEM-1400EX, JEOL, Japan). The density of myelinated axons was determined from the toluidine blue stained image. The thickness of myelin sheaths and the diameter of myelinated nerve fibers was determined from the TEM image. For each section, three random images were selected and quantitatively analyzed with ImageJ.

For immunofluorescence staining (IF), at 12 weeks postoperatively, the nerve grafts were fixed in 4 % PFA, and the samples were then cut into sections longitudinally through a freezing microtome (CM1950, Leica, Germany). Staining steps reference to the previously studies, then IF were scans by using a Zeiss Axio Scan. Z1 scanner (Carl Zeiss, Germany), and the images were processed using Zen 3.3 (Blue edition) software (Carl Zeiss, Germany). Three images randomly selected from the rats' section to calculate the average of each index for analysis. The antibodies used were listed in Table S2.

2.10. Statistical analysis

The data were processed through ImageJ, Prism 9 (GraphPad Software), Origin software (Origin Lab), Adobe illustrator (Adobe Inc). Data are presented as mean ± standard deviation (SD) and statistically analyzed using one-way analysis of variance (ANOVA) followed by Tukey's post hoc test (equal variances) or Dunnett's T3 post hoc test (unequal variances) with the SPSS 22.0 software. Values of $p < 0.05$, 0.01, and 0.005 were considered statistically significant, high significant, and extreme high significant, respectively.

3. Results

3.1. Preparation and characterization of the blow-spun collagen nanofiber membrane and nerve conduit

To confirm the feasibility and advantage of blow-spinning technique

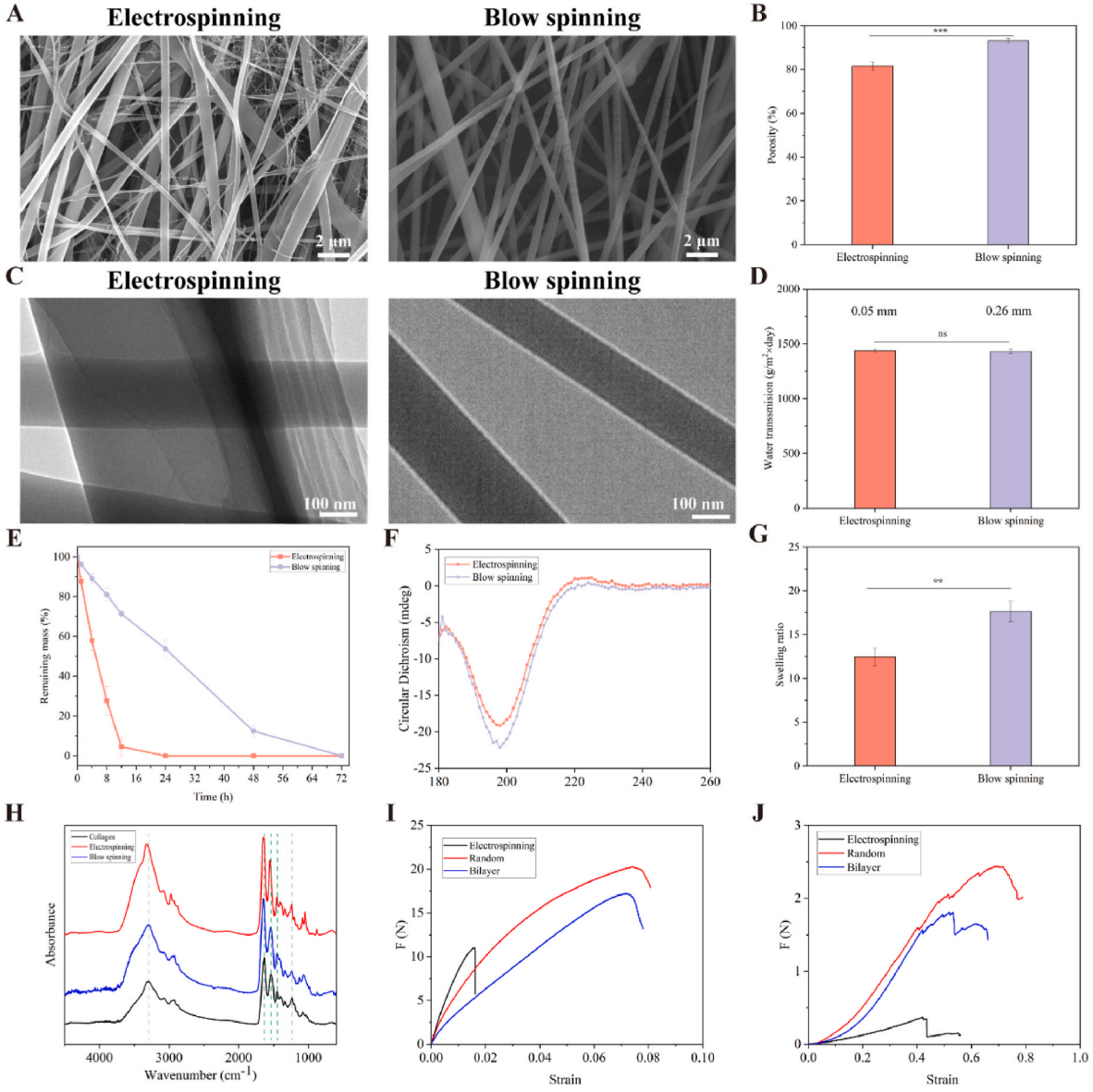

Fig. 2. Characterization of electrospun and blow-spun collagen nanofibers membranes. (A) The SEM images of electrospun and blow-spun collagen nanofibers. (B) Calculated porosity of the collagen membranes prepared by electrospinning and blow-spinning. (C) The TEM images of electrospun and blow-spun collagen nanofibers. (D) The water vapor transmission rate of collagen membranes. (E) *In vitro* degradation of the collagen membrane. (F) CD spectra of electrospun and blow-spun collagen membranes. (G) The swelling ratio of the collagen membranes. (H) FTIR spectrum of the natural collagen, electrospun and blow-spun collagen. (I) The stress-strain curves of dry collagen nerve conduits. (J) The stress-strain curves of wet collagen nerve conduits.

on collagen nanofiber fabrication for NGC development, two types of collagen nanofibers prepared respectively by blow-spinning and electrospinning were compared. HFIP was used as the solvent for electrospinning. In the blow-spinning process, acetic acid solution was utilized instead of HFIP to prepare collagen nanofibers. The typical SEM and TEM images revealed that both the electrospinning and blow-spinning could fabricate uniform collagen nanofibers. The electrospun collagen fibers had uneven fiber thickness with ultrafine filaments entangled (Fig. 2A and C). In contrast, the collagen fibers produced through blow-spinning demonstrated improved uniformity, implying its good spinnability. Moreover, the SEM images indicated that the blow-spinning membranes exhibited larger pore sizes and a more porous structure. Quantitative calculation of porosity corroborated these findings, demonstrating that the blow-spinning collagen membranes possessed higher porosity, which is advantageous for the transfer and metabolism of growth factors (Fig. 2B). Increased porosity suggests enhanced permeability and breathability, prompting us to assess the water vapor transmission rates of the collagen membranes as a measure of their breathability. Due to challenges in achieving consistent thickness with electrospun collagen membranes compared to the blow-spinning membranes, we employed a fixed volume and concentration of spinning solution (10 mL) for the comparison. The results revealed a minimal difference in WVTR between the electrospun membranes (thickness: 0.05 mm) and the blow-spun membranes (thickness: 0.26 mm) (Fig. 2D). It is essential to note that this outcome was obtained under different conditions thickness the membranes. Generally, as thickness increases, the transfer of substances becomes more difficult. Consequently, it can be inferred that at the same thickness, the blow spinning collagen membranes exhibit superior water vapor permeability. Furthermore, we also observed an increased swelling property in the blow-spun collagen membrane in comparison to electrospun one, which has a close correlation with their porosity features (Fig. 2G).

To increase the degradation period, chemical crosslinking was applied. Notably, the blow-spun collagen membranes after cross-linking exhibited an extended degradation time *in vitro* (Fig. 2E), which may be attributed to more sufficient crosslinking due to the fluffier and spongier structure and increased porosity of the blow-spun fiber membranes with increased penetration of crosslinking reagent. In addition, the collagen structures in different solvent after spinning were also evaluated. Recent research has revealed that fluorinated alcohols have a severe detrimental effect on the tertiary structure of collagen [24]. In order to explore whether blow-spun fibers in an acetic acid system could better preserve the structure of collagen protein, we employed three analyses: proton nuclear magnetic resonance spectroscopy, circular dichroism, and Fourier-transform infrared spectroscopy (Fig. 2F and H, and S1). The results obtained from the three assays consistently indicated that utilizing an acetic acid system as solvent was more effective in maintaining the integrity of the collagen protein structure.

As a nerve conduit, squeezing caused by frequent stretching and contraction of surrounding tissues during the host's movement cannot be avoided. Therefore, the mechanical properties of the conduit in dry and wet should be considered. To evaluate this aspect, we compared electrospun random conduit with blow-spun random and bilayer conduit after cross-linking. Our findings indicated that the conduit prepared via blow spinning exhibited superior tensile strength and ductility, which can be attributed to their fluffy and random structure (Fig. 2I). The random conduit characterized by high disordered nanofibers could bear greater force during the stretching process compared with electrospun or bilayer one. The bilayer conduit displayed lower tensile strength compared to the random structure, but still outperformed the electrospun group. To simulate the *in vivo* environment, we conducted tests on the conduit s in wet (Fig. 2J). Although a noticeable reduction in tensile strength was observed, these membranes demonstrated improved extensibility, indicating their capacity to withstand significant deformations under normal physiological forces. Similarly, both types of conduits prepared via blow spinning exhibited enhanced tensile strength and ductility. These findings consistently demonstrate the feasibility and superiority of utilizing blow-spinning as a substitute for electrospinning in the fabrication of collagen nanofiber conduit.

To create a more uniform blow-spun collagen membrane, multi-needle spinning process was applied (Fig. S2). It revealed that the use of a multi-needle spinning approach significantly increased the thickness uniformity of the membrane on both sides of the drum, resulting in a more even overall membrane than single-needle spinning (Fig. S3). This substantial enhancement greatly improved the collection efficiency. Besides, the injection rate of the syringe was identified as a critical parameter that could significantly influence the spinning characteristics and continuity of the solution. Using a high-speed camera, we investigated the blow spinning process of collagen solutions injected at different rates (Fig. S4, Video S1–S3). At an injection rate of 2.5 mL/h, it was observed that the solution rapidly formed a jet under the effect of gas shear, but due to the extrusion speed of the solution being lower than the volatilization rate, the spraying jet was discontinuous. When the injection rate was increased to 5 mL/h, the extrusion speed of the solution at the needle tip balanced with the volatilization rate due to the higher injection speed, allowing for the formation of a stable jet under the effect of gas shear, ensuring continuous fiber formation.

Based on the aforementioned findings, we prepared fluffy collagen fiber sponges and collagen met using the multi-needle blow spinning approach (Fig. S5). By altering the drum's collection speed, we obtained both random and oriented collagen fibers (Fig. 3D). Subsequently, the collected collagen membranes were rolled into conduits (Fig. 3A, B, 3C). The typical SEM images of the cross-sections and surface structure of random and bilayer conduits were shown in Fig. 3F, G, 3H, and 3I. To assess the suturing properties of the conduits, we simulated an *in vivo* wet environment by immersing them in PBS. We then compared the suturing capabilities of dry conduits with those that had been exposed to moisture. The results demonstrated that both types of conduits effectively supported a 25 g weight during suturing (Fig. 3E and J).

3.2. *In vitro cell culture on the blow-spinning collagen membranes*

From a perspective of NGCs, the pore features are crucial for the performance of the tubes, which allow sufficient O_2 and nutrition diffusion and also confine a microenvironment to avoid non-neural tissues invasion, thus providing unobstructed path for axonal sprouting and maturation. Therefore, in this study, we simulated the *in vivo* condition of nerve conduits to examine if the fibroblasts could easily invade across the porous walls into the tubes. The L929 cells were cultured on the surface of the blow-spun collagen membrane for up to three days. After immunofluorescence staining of rhodamine-phalloidin, the L929 cells were imaged by CLSM in 3D. It can be seen that the L929 cells had very good adhesion and spreading on the membrane, indicating its excellent cytocompatibility. Besides, the 3D reconstruction images showed the cells on the blow-spun membranes migrated a little deeper than those on electrospun membranes, which was reasonable because of the spongier structure of the blow-spun membranes. Nevertheless, the L929 cells dominantly attached on the surface region and did not infiltrate into the inside of the blow-spun collagen membrane (Fig. 4A and S6). This suggested that blow-spun fibers could confine the defected space. More than that, the multi-layer structure of the tube formed by membrane rolling will further block cell invasion.

Additionally, *in vitro* cell culture of RSCs on the electrospun and blow-spun membranes were evaluated. Again, we observed good adhesion and spreading on both membranes, indicating the good biocompatibility the collagen membranes (Fig. 4B and S7). To investigate cell functions of RSCs on different membranes, we assessed the expression of Schwann cell-related genes to compare electrospun and blow-spun collagen membranes. The level of myelination of Schwann cells plays a pivotal role in peripheral nerve regeneration. Hence, we assessed five Schwann cell specific genes: S100, myelin basic protein

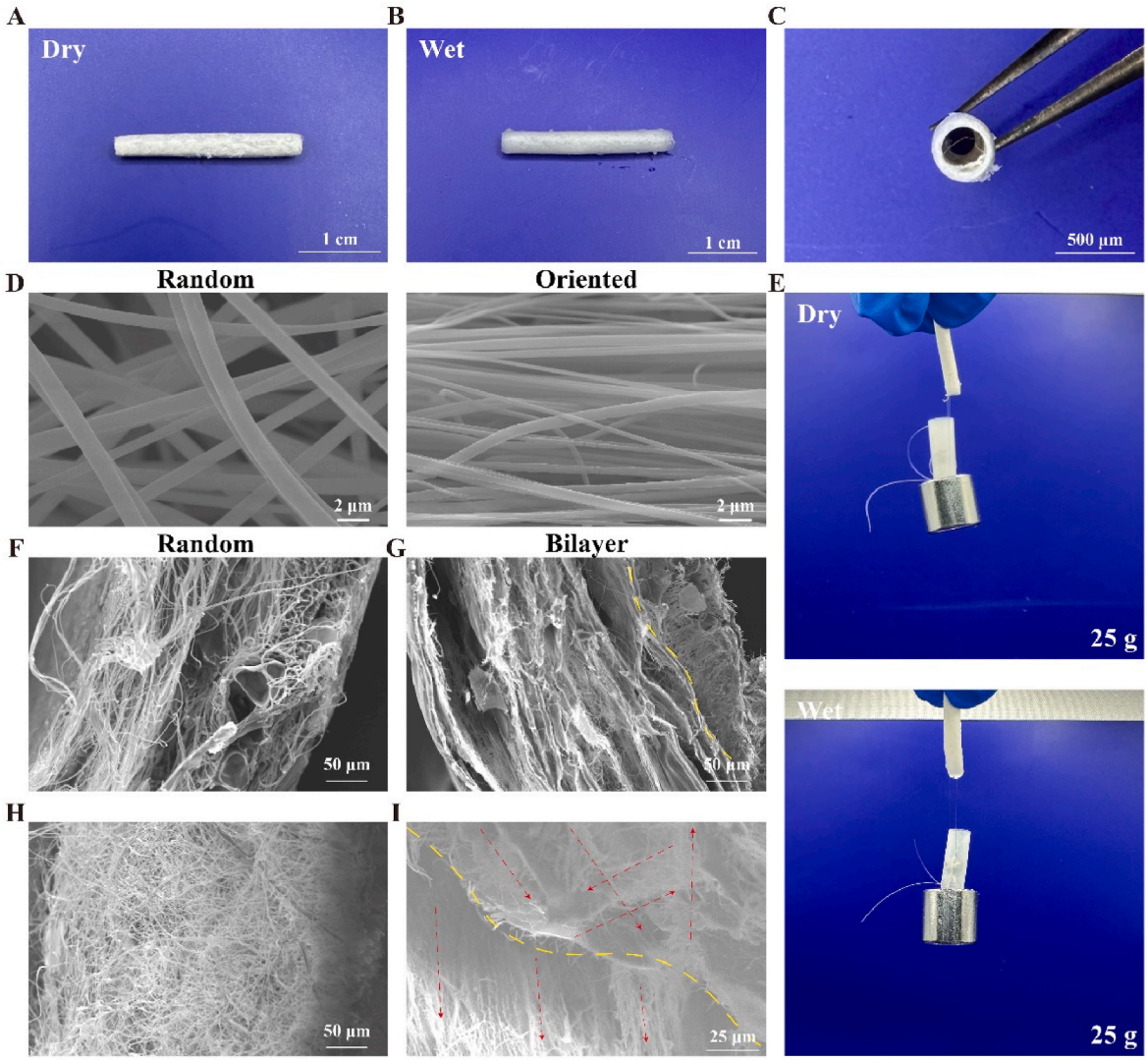

Fig. 3. Characterization of blow-spun collagen nanofiber tubes. (A) Dry collagen NGC. (B) Wet collagen NGC. (C) Cross-sectional view of the collagen NGC. (D) The SEM images of random and oriented collagen nanofibers. (E) Suturing performance of dry and wet collagen NGCs. (F) The cross-sectional SEM images of random NGC. (G) The cross-sectional SEM images of bilayer NGC. (H) SEM images of the longitudinal section of random NGC. (I) SEM images of the longitudinal section of the bilayer NGC.

(MBP), peripheral myelin protein (PMP22), neuropilin 2 (NRP2), and Myelin Protein Zero (P0). Moreover, it's worth noting that immature Schwann cells typically express neuronal cellular adhesion molecules (NCAM) and low-affinity nerve growth factor receptor (p75) during their developmental stages [25]. The results notably revealed that the myelination was significantly promoted in RSCs cultured on blow-spun collagen membranes with increased gene expression of S100, MBP, PMP22, NRP2 and decreased expression of NCAM and P75 in comparison to the electrospinning group (Fig. 4C). Moreover, the expressions of typical neurotrophic growth factors including nerve growth factor (NGF), brain-derived neurotrophic factor (BDNF), ciliary neurotrophic factor (CNTF), glial cell derived neurotrophic factor (GDNF), insulin-like growth factor-2 (IGF-2), vascular endothelial growth factor (VEGF), and transforming growth factor beta (TGF-β) were also examined, which were all upregulated (Fig. 4D). These results indicated the blow-spun collagen membranes provided a favorable matrix for RSCs growth, maturation, and growth factors secretion.

3.3. Oriented membrane regulated gene expression in Schwann cell and macrophages

It's widely accepted that aligned structure could accelerate neurite outgrowth and nerve regeneration [8]. In this study, we designed a bilayer structure with aligned collagen nanofibers along the long axis of the NGCs. Therefore, we assessed cell proliferation of RSCs using the CCK-8 assay and typical gene expressions using RT-PCR to confirm the ability of the aligned collagen nanofibers on cell alignment, growth, and maturation. The CCK-8 assay clearly demonstrated that the Oriented group exhibited superior cell proliferation compared with Random group (Fig. 5A). Furthermore, the cytoskeleton staining confirmed the organized alignment of RSC in response to the well-oriented structures within the material (Fig. 5B). This alignment is particularly advantageous for promoting axonal extension and growth in cases of peripheral nerve injury. The gene expression of Schwann cell including S100, MBP, PMP22, NPR2, NGF, BDNF, CNTF, and IGF-2, cultured on different collagen membranes for three days were examined (Fig. 5C). The results revealed significantly higher gene expression of S100, MBP, PMP22, and NPR2 in the Oriented group compared with the Random group, highlighting the positive influence of the oriented structure on myelination.

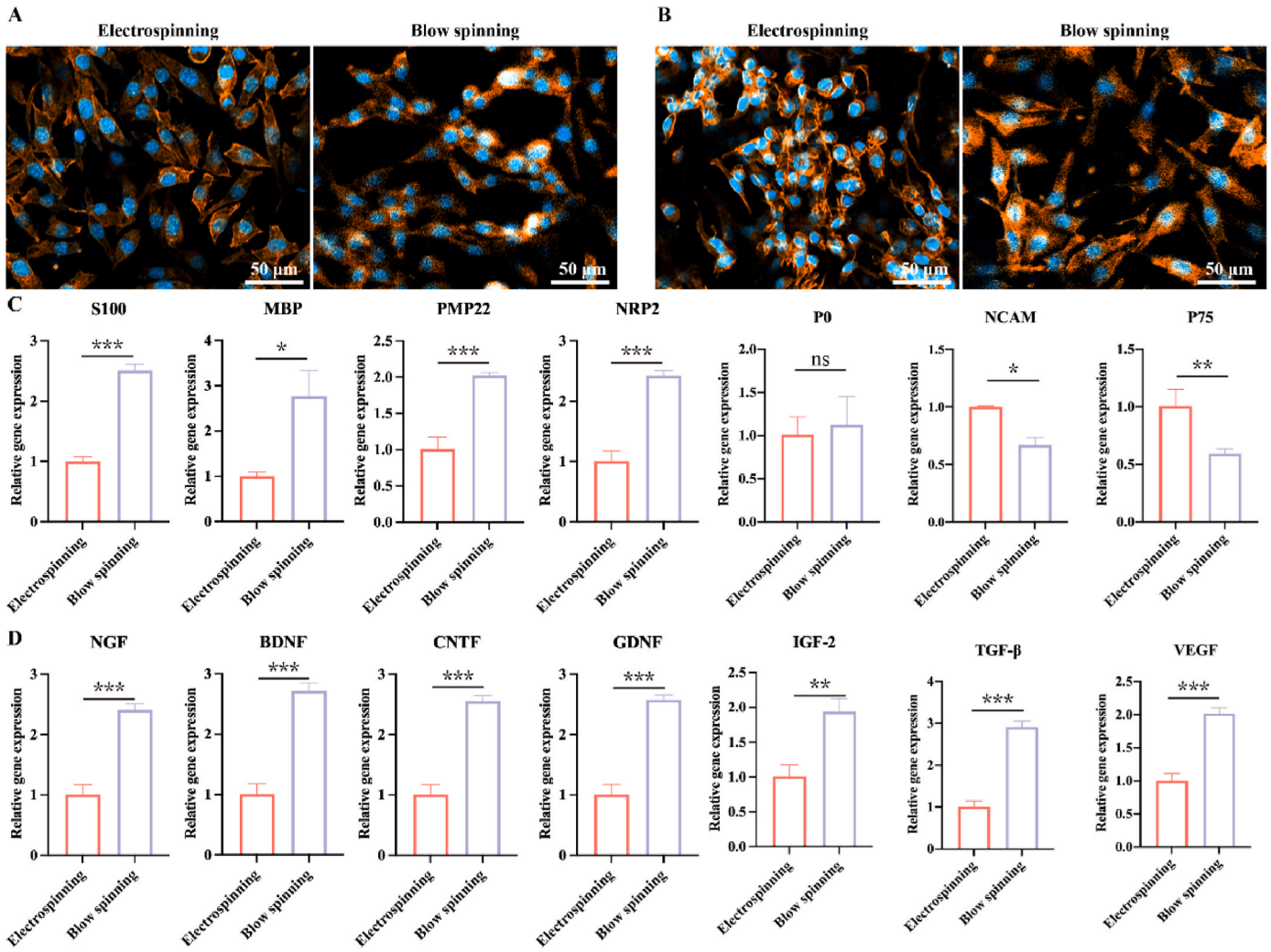

Fig. 4. Cell morphology and gene expression on electrospun and blow-spun collagen membranes. (A) Representative confocal microscopy images of L929 stained with rhodamine-phalloidin on electrospun and blow-spun collagen membranes on day 3. (B) Representative confocal microscopy images of RSCs stained with rhodamine-phalloidin on electrospun and blow-spun collagen membranes on day 3. (C) The real-time qPCR analysis of RSCs differentiation-related gene expressions after 3 days (n = 3). (D) The real-time qPCR analysis of neural and growth-related factor gene expressions of RSCs after 3 days (n = 3).

Moreover, the Oriented group displayed superior gene expression of the neurotrophic factors NGF, BDNF, CNTF, and IGF-2 compared with the Random group. All these findings provided additional evidence that the oriented structure promoted the secretion of neurotrophic factors, thereby enhancing the overall neurogenic environment.

RAW264.7 cells were polarized with LPS to simulate the inflammatory response after *in vivo* injury, thus evaluating the immunomodulatory properties of blow-spun oriented collagen (Fig. 5D). In activated macrophages, the expression of inflammation-related genes CD86 and IL-6 showed a decreasing trend in both Random and Oriented groups. Moreover, the expression of anti-inflammatory genes IL-10 and Arg1 significantly increased in both groups. These results suggest that fluffy blow-spun collagen may be more beneficial in helping tissues resist inflammation and that the oriented topographic structure plays an important role in the anti-inflammatory response.

3.4. Motor functional recovery

Four groups of nerve grafts (Chitosan, Random, Bilayer, and Autologous) were implanted to bridge the 15-mm-long transected sciatic nerve gaps in rat to evaluate the impact of the nerve conduit on nerve regeneration *in vivo* (Fig. S8). After peripheral nerve injury, the restoration of neural electrical signal transmission and motor function is the most important indicator, especially for long-distance nerve injuries. In order to evaluate functional recovery after peripheral nerve injury, compound muscle action potential (CMAP) of the gastrocnemius muscle was recorded at 12 weeks post-surgery. Additionally, we used commercially available chitosan conduits as a control group to assess the feasibility of the blow-spun conduit commercialization. Fig. 6A showed representative electrophysiological images of the injured side in each group. The CMAP amplitude of chitosan group was significantly lower than all other groups, while the bilayer group showed the highest CMAP compared with the chitosan and random groups, no significant difference with the autograft group ($p = 0.0757$). Additionally, there was a slight difference between the Random and Bilayer groups ($p = 0.0311$) (Fig. 6B).

Furthermore, the recovery of hind limb movement was further evaluated through catwalk analysis. The sciatic functional index (SFI) is an indicator of the degree of nerve dysfunction, ranging from 0 to 100, with 0 indicating normal function and 100 indicating complete dysfunction. As time increased, motor function gradually recovered in all groups. The chitosan group showed significantly poorer recovery compared with the other groups. Additionally, at 12 weeks post-surgery, there was no significant difference between the bilayer and autograft groups (Fig. 6C). These results indicate that the bilayer group contributes to the improvement and good restoration of motor function. The

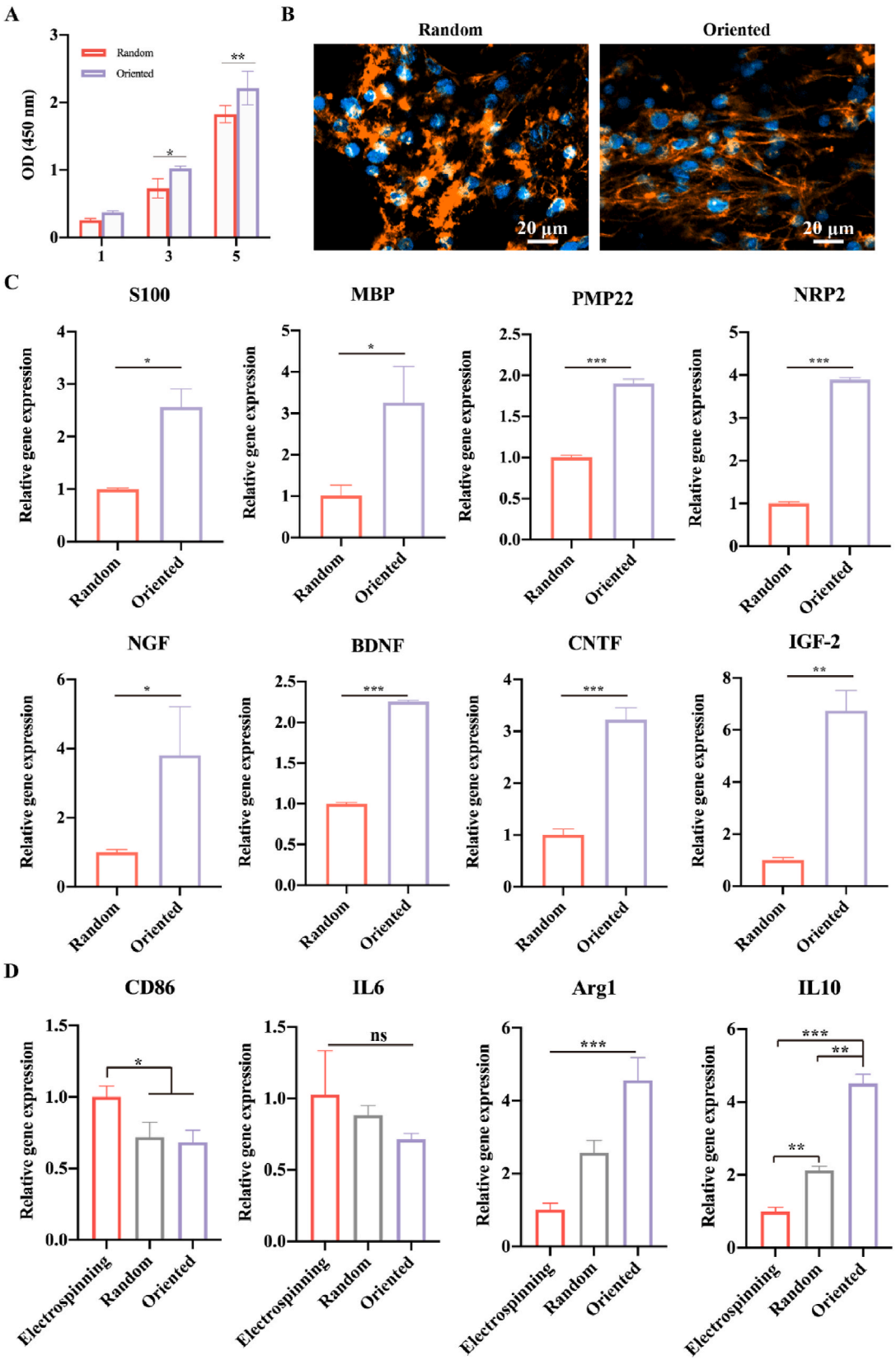

Fig. 5. Schwann cell morphology and gene expression on random and oriented collagen nanofiber membranes. (A) CCK-8 assay of SCs proliferation on membrane after 1, 3, 5 days of culture (n = 3). (B) Representative confocal microscopy images of SCs stained with rhodamine-phalloidin on random and oriented membrane on day 3. (C) The real-time qPCR analysis of gene expressions of SCs after 3 days (n = 3). (D) The real-time qPCR analysis of gene expressions of RAW 264.7 after 3 days (n = 3).

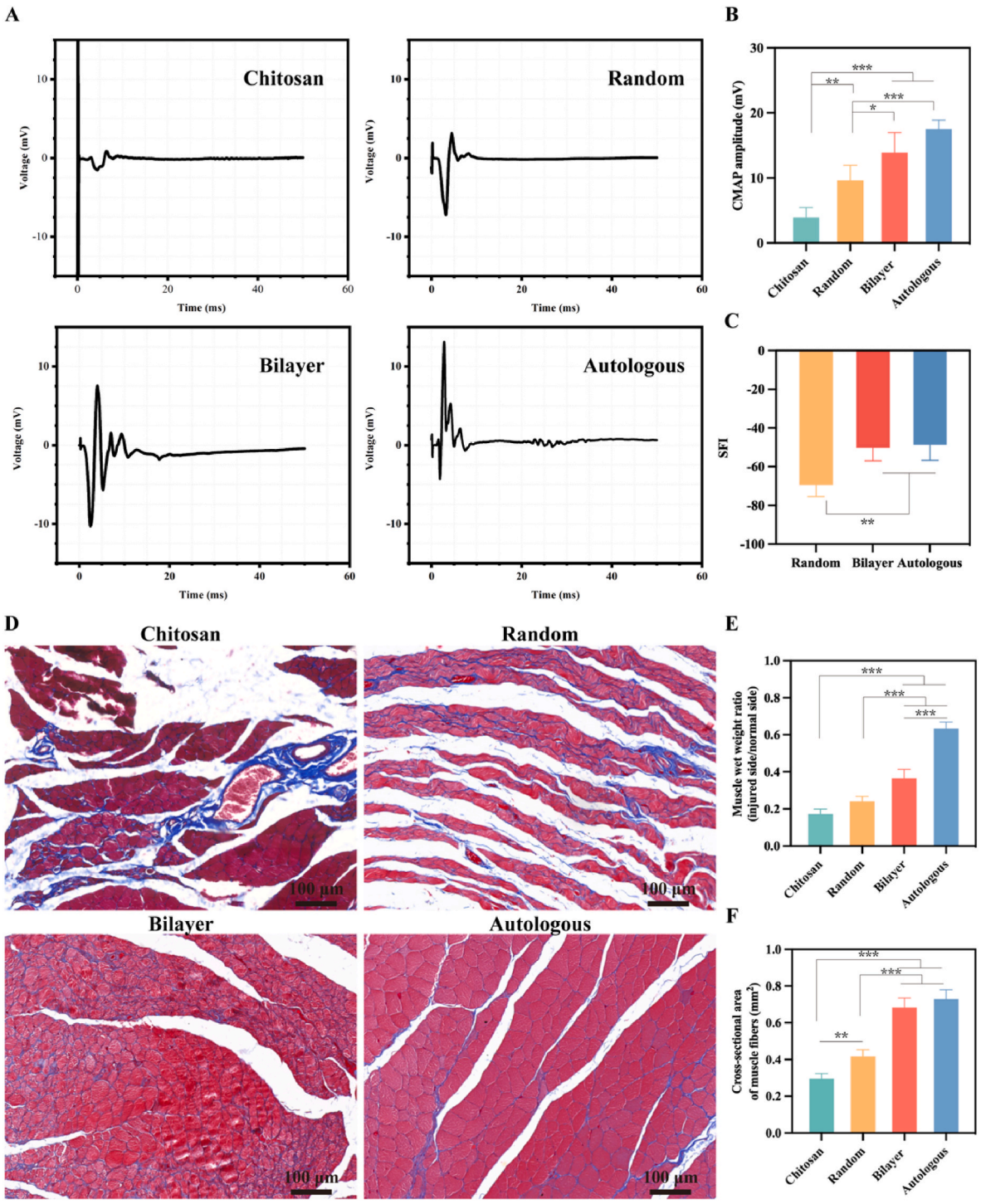

Fig. 6. Assessment of electrophysiological efficacy and recuperation of motor function 12 weeks after the surgical procedure. (A) Electrophysiological performance was assessed by recording Compound Muscle Action Potentials (CMAP) at the injured site, with electrical stimulation administered at both the proximal and distal nerve stumps. (B) CMAP amplitude at the injured site was statistically analyzed. *P < 0.05 and ***P < 0.001 (n = 5). (C) Motor functional recovery was evaluated over a 12-week period using Sciatic Functional Index (SFI) values. *P < 0.05 and ***P < 0.001 (n = 5). (D) Transverse sections of muscles from the injured limbs were subjected to Masson's trichrome staining. (E) Muscle wet weight ratios of the lesioned side of rats were statistically analyzed relative to the non-lesioned side. ***P < 0.001 (n = 5). (F) The average cross-sectional areas of muscle fibers were also statistically analyzed. ***P < 0.001 (n = 5).

structural design of the conduit led to the differences between the two groups, while the differences from chitosan may stem from differences in fiber structure and porosity. The fiber structure can induce cell alignment and promote nerve regeneration, and the conduit designed through the blow-spinning process has the characteristics of appropriate porosity, facilitating the delivery and metabolism of nutritional factors in the injury microenvironment.

At 12 weeks post-surgery, rats were euthanized, and the wet weight ratio of the gastrocnemius muscle was calculated. We found that, although there was still a significant difference between the bilayer group and the autograft group, the recovery effect of the bilayer group was superior to that of the commercially available chitosan and Random

groups (Fig. 6E). Additionally, we analyzed the area of the gastrocnemius muscle fibers through Masson staining to assess muscle atrophy (Fig. 6D). We found no significant difference between the bilayer and autograft groups, while the commercial chitosan and Random groups showed an obvious decrease in the area of gastrocnemius muscle fibers (Fig. 6F). We speculate that this may be due to the oriented fiber structure in the bilayer group, which promotes the recovery of nerves and surrounding tissues, resulting in better muscle fiber repair. Although the increase in muscle fiber area indicates the effectiveness of muscle recovery, 12 weeks of repair time is not sufficient to fully compensate for the lost muscle. Nonetheless, our experimental results still suggest the great potential of the Bilayer conduit prepared through blow-spinning to replace commercial products.

3.5. Axonal regeneration and re-myelination

After 12 weeks post-implantation, the regenerated nerves were harvested and sectioned transversely. The cross-sections from the middle site were observed using both toluidine blue staining and TEM to analyze the degree of axonal regeneration and myelination. Toluidine blue staining images showed that all groups exhibited regenerated myelinated nerve fibers (Fig. 7A). The results of quantitative analysis indicated that both the autograft (12979.8 ± 2385.0 nerves/mm^2) and bilayer groups (10942.2 ± 855.1 nerves/mm^2) were significantly higher than the random group (6428.7 ± 1336.3 nerves/mm^2) and chitosan group (5400.2 ± 638.7 nerves/mm^2), although the density of the bilayer group was lower than that of the autograft group, there was no significant difference between the two ($p = 0.0807$) (Fig. 7C). TEM images revealed additional details about the extent of myelination and maturity in the regenerated nerves, as indicated by parameters such as myelin thickness and axon fiber diameter (Fig. 7B). The autograft group showed significantly larger axon diameter (3.71 ± 1.54 μm) and myelin thickness (0.80 ± 0.33 μm) compared with the other three groups. Similarly, the bilayer group exhibited significantly larger axon diameter (3.16 ± 1.23 μm) and myelin thickness (0.61 ± 0.10 μm) than those observed in the random group (2.69 ± 0.99 μm, 1.59 ± 0.35 μm) and chitosan group (0.42 ± 0.16 μm, 0.29 ± 0.03 μm) (Fig. 7D and E). Subsequently, the g-ratio, measured by calculating the ratio of axon diameter to fiber diameter based on both the circumference and diameter, was used as a measure of the degree of myelination in nerve fibers. It represents the proportion of the nerve fiber composed of the myelin sheath, which is a lipid insulating layer that wraps around the axon and helps increase the conduction velocity of electrical signals along the nerve fiber. In general, the optimal value of the g-ratio in healthy peripheral nerves is typically

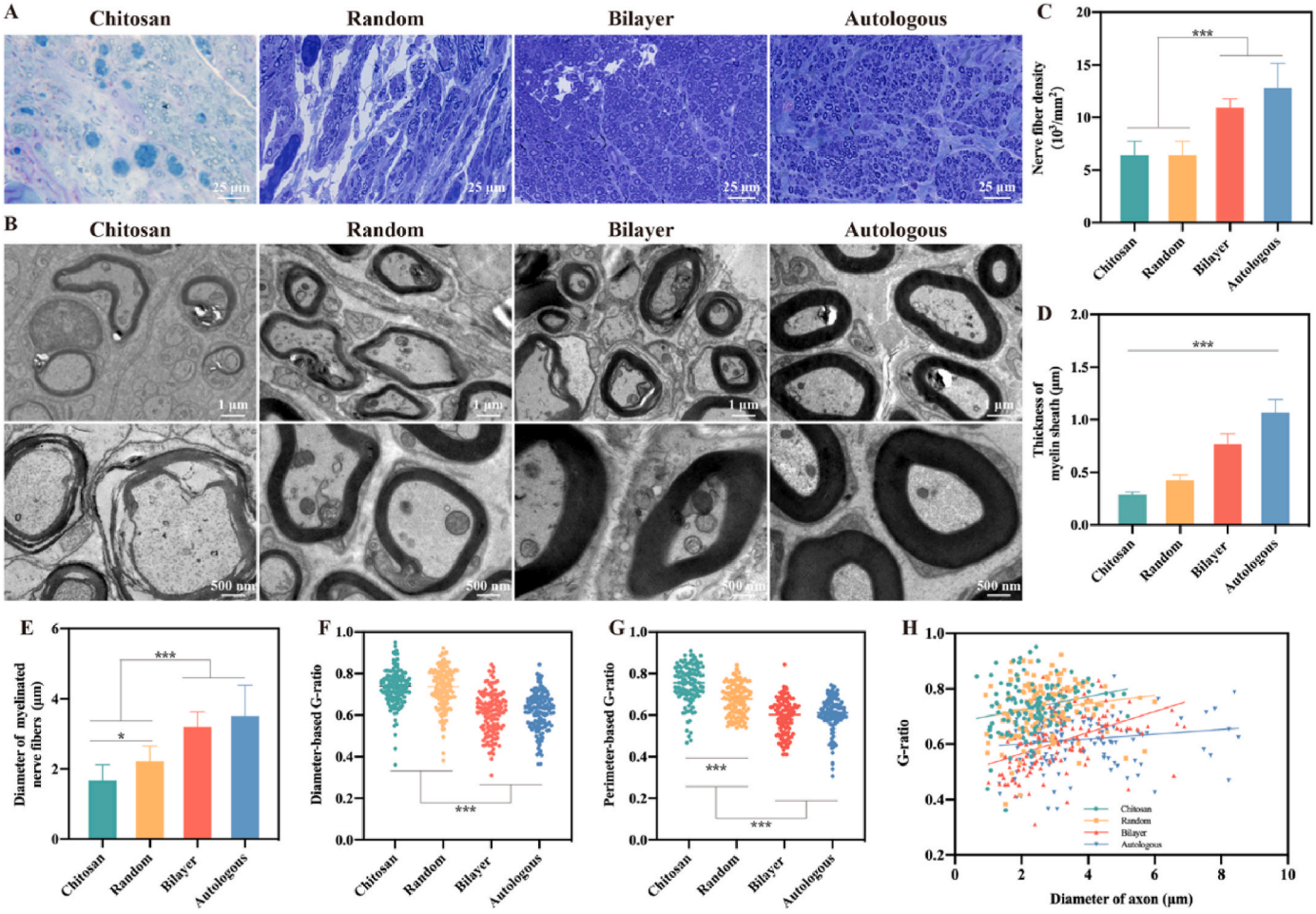

Fig. 7. Assessment of regenerated nerve fibers was conducted at the distal site of nerve grafts 12 weeks after the surgical procedure. The evaluation included (A) examination of toluidine blue-stained images and (B) transmission electron microscopy (TEM) images of transverse sections taken from the middle site of the harvested nerve grafts. (C) Statistical analysis was performed on the density of myelinated nerve fibers, which was quantified from images stained with toluidine blue. (D) Statistical analysis was conducted on the diameter of myelinated nerve fibers, which was quantified from TEM images. (E) Statistical analysis was carried out on the thickness of the myelin sheath, which was quantified from TEM images. (F) Statistical analysis was undertaken on the diameter-based g-ratio. (G) Statistical analysis was executed on the perimeter-based g-ratio. (H) A scatter diagram was plotted to show the relationship between the g-ratio and axon diameter. Significance levels were indicated as *$P < 0.05$ and **$P < 0.01$, based on a sample size of 3 ($n = 3$). (For interpretation of the references to color in this figure legend, the reader is referred to the Web version of this article.)

around 0.6 [26].

In this study, the diameter-based g-ratio values for the bilayer group (0.61 ± 0.1) and autograft group (0.62 ± 0.09) were significantly lower than the random group (0.73 ± 0.1) and chitosan group (0.74 ± 0.09), indicating that the oriented structure enhanced myelin formation around axons, consistent with the *in vitro* results (Fig. 7F). A similar trend was observed for the circumference-based g-ratio values. The bilayer group (0.59 ± 0.09) and autograft group (0.60 ± 0.08) had significantly lower g-ratio values than the random group (0.67 ± 0.08) and chitosan group (0.75 ± 0.09) (Fig. 7G). Scatter plots of the g-ratio analysis revealed that the autograft group exhibited a higher number of larger-diameter myelinated fibers, followed by the bilayer group, while the random group had much smaller-diameter myelinated fibers (Fig. 7H). Additionally, we observed a crossover in the fitting curves of the bilayer and autograft groups, indicating that the bilayer group had a higher proportion of smaller-diameter myelinated fibers with lower g-ratio values, which further supported their growth. The random group consistently exhibited higher g-ratio values compared with both groups, regardless of fiber diameter. These results demonstrate that the bilayer conduit structure enhances nerve regeneration.

It is important to highlight that the extent of myelination in Schwann cells and the connectivity of neurons play a crucial role in the transmission of nerve signals, a factor directly linked to the recovery of motor function. To gain deeper insights into whether directional nerve conduits contribute to enhancing the myelination of sciatic nerve fibers and the extent of axon regeneration, we conducted dual immunofluorescence staining for S100 and 200 kDa subunit of neurofilament (NF200), serving as markers for Schwann cells and neuronal cell, respectively (Fig. 8). At the 12-week post-surgery, when compared with the random group, both the bilayer and autograft groups displayed robust and widespread axon regeneration. In the bilayer group, there were observable patterns of alignment among neuronal cells, whereas the autograft group exhibited a more orderly and longitudinally oriented arrangement of NF200-stained cells. In contrast, the random group exhibited only a limited presence of S100-positive signals, while the bilayer group displayed a significantly greater number, in line with the findings from our cellular experiments. This strongly suggests that the bilayer group has the potential to promote axon regeneration and increase the population of Schwann cells in comparison to the random group.

4. Discussion

The reconstruction of a nerve-favorable microenvironment by using NGCs has already become a very promising strategy for clinical treatment for PNI. Currently, no available NGC product has been developed that can compare with autograft transplantation. How to design an ideal NGC that is considered as the first choice instead of autograft is a key issue for PNI repair [27,28]. Given a myriad of factors that bring the challenges to neural regeneration, such as excessive immune responses, inadequate vascular development, suboptimal energy metabolism, oxidative stress from reactive oxygen species, and disruption of neural

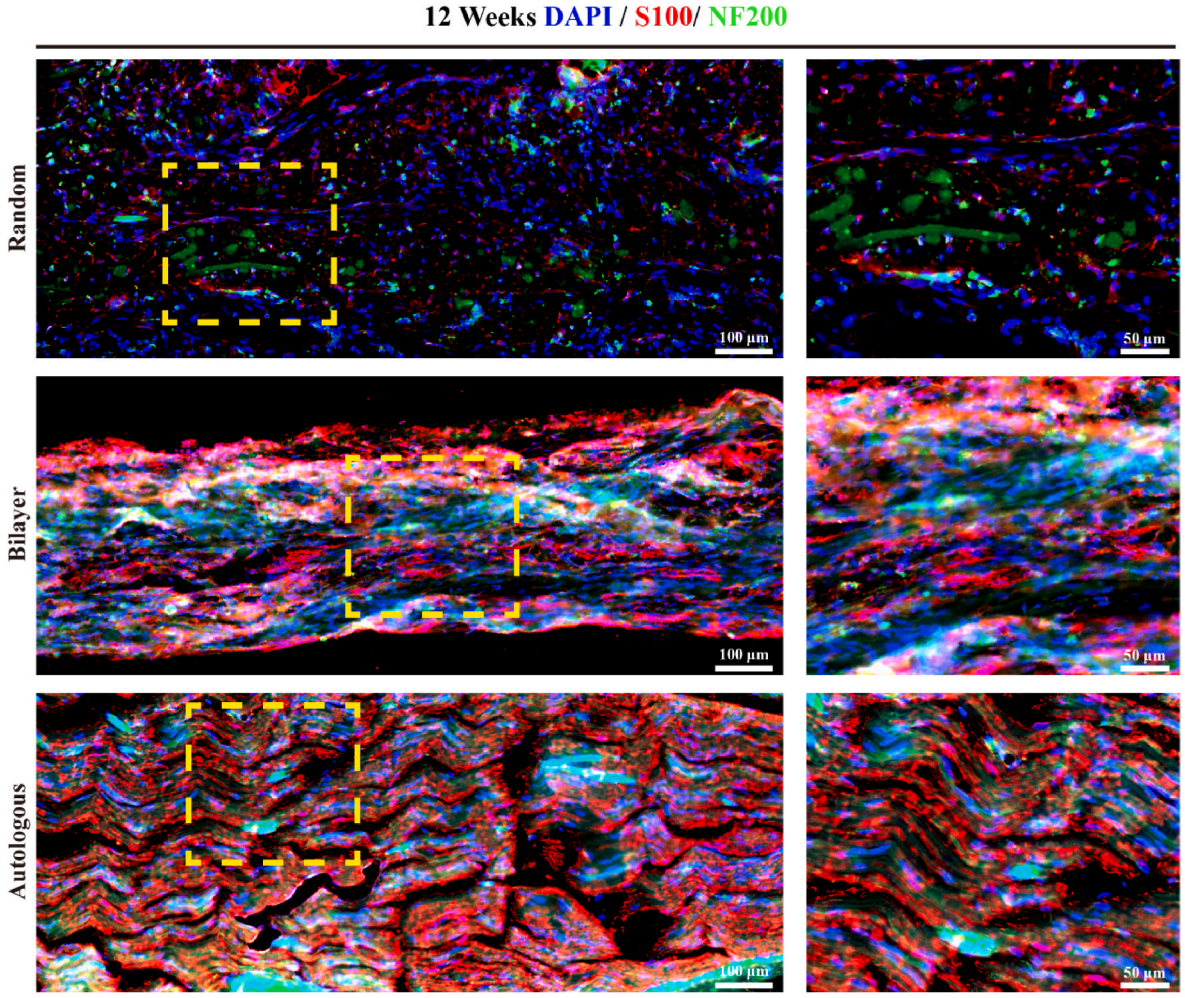

Fig. 8. Immunofluorescence staining (IF) was performed on the axons expressing S100 and NF200 (neurofilament 200) at the middle segment of the harvested nerve grafts 12 weeks after the surgery.

electrical signaling, a multifaceted approach is necessary to facilitate effective regeneration and repair. Recent advances in multimodal repair strategies that combine the intricacies of nanomaterial-based topographic structures, targeted biochemical signaling, and calibrated external physical stimuli to synergistically refine the intraluminal environment have shown promising potentials in enhancing neural regeneration [28]. In this context, the presence of an ideal tubular scaffold remains crucial for ensuring the long-term effectiveness of the neurogenic intraluminal cues. Although the majority of commercially available NGC products manufactured in the format of hollow tube have been in a long-term application in clinical practice, they are not entirely satisfactory, lacking of sufficient radial support in wet, controllable degradation behavior, aligned nano-topography, or suturing performance. Therefore, it is still crucial to develop a novel hollow tube, the main component of NGCs that is considered as the first scaffold for guiding nerve regeneration.

In fact, the fabrication processing often has a direct impact on the overall performances of the NGCs. For example, the freeze-drying spongy scaffolds have poor mechanical properties, especially in wet, which cannot ensure unblocked tunnel for nerve regeneration. And the electrospinning method can fabricate nanofibrous membranes for rolling into multilayers of tubes, while they always have limited porosity and pore size for diffusion. In fact, these physiochemical properties are quite important for the tubular scaffolds to bridge the peripheral nerve defects and promote axonal regrowth. In this study, we successfully developed a new processing based on blow-spinning technique to fabricate collagen nanofibrous membranes. The entire production process has no limit on biomaterial characteristics, the solvent type, surrounding environment, and collector geometry [29]. In addition, its commercial scalability with low equipment costs and high production efficiency is also one of the most attractive advantages of blow-spinning technique [13]. Most importantly, the blow-spun nanofiber membrane exhibits a fluffy and spongy structure, facilitating efficient nutrient delivery and metabolic exchange both within and outside the conduit, which also contributes to the penetration of crosslinking reagent for sufficient chemical crosslinking. At the same time, the bilayer structure with oriented nanofiber inner layer and random nanofiber outer layer enhances the mechanical properties of the conduit both in dry and wet conditions, displaying good radial support and suturing performance, while providing oriented nano-topography cue simultaneously.

The optimized physiochemical properties distinctly contributed to the biological performances of the blow-spun NGC for PNS regeneration. Through *in vitro* experiments, we observed induced cellular alignment and axonal growth, attributable to the oriented topological structure. Furthermore, the oriented structure promotes myelination and enhances the secretion of neurotrophic factors. These *in vitro* results suggest that the blow-spun collagen fibers may be helpful for reconnecting disrupted neural electrical signal transmission. In addition, we found that oriented blow-spun collagen fibers can reduce the gene expression of inflammation-related factors and significantly upregulate the gene expression of anti-inflammatory factors, which may be associated with the oriented topological structure [30]. In brief, the *in vitro* cellular results indicate that oriented blow-spun collagen fibers exhibit great potential in promoting neural regeneration. Consequently, we further evaluated their efficacy in neural injury repair using a rat sciatic nerve injury model. The *in vivo* results showed that rats implanted with nerve conduits containing an inner oriented structure exhibited faster axonal regeneration, better motor functional recovery and conduction of electrical signals, which were comparable to the autograft transplantation group.

The degradation of blow-spun collagen membranes is crucial for their regenerative performance as neural conduits [31]. In the field of peripheral nerve regeneration, rapid degradation of tube materials can potentially undermine their role in facilitating nerve regeneration and mechanical support, while slow degradation may also have harmful effects on newly regenerated nerve tissues. Ideally, the conduits should degrade within a period of 2–6 months. *In vitro* degradation experiments indicated the good degradability of the crosslinked collagen membranes in the presence of enzymes. Furthermore, *in vivo* evaluations also confirmed the acceptable degradation behavior of the blow-spun collagen tubes at 6 and 12 weeks after surgery. However, the degradation rate *in vivo* could be further optimized by extending the duration to provide better guidance and mechanical protection. Additionally, for clinical applications, the degradation rate needs to be fine-tuned, taking into account the disparity in regeneration rates between humans and rats. Furthermore, the degradation of the NGCs will inevitably affect their mechanical properties. The degradation characteristics of our conduits can be adjusted by modifying conduit geometry (such as the compactness and wall thickness of the rolled conduits), optimizing the cross-linking process (involving cross-linking agents and their application duration), and utilizing composite materials [32,33].

In this study, motor functional recoveries were achieved and evaluated in the repair of rat sciatic nerve injury. It is also important to investigate the sensory functional recovery under the guidance of collagen tubes. The hot plate test is commonly used to assess the recovery of sensory neural systems, including pain and touch [34,35]. However, we contend that direct evaluation of sensory function recovery using techniques like the hot plate test, is not entirely accurate. The outcomes of such tests are inevitably influenced by both sensory and motor functional recoveries. Consequently, this overlap compromises the specificity and rigor required for a precise assessment of sensory function recovery, suggesting a need for more refined or targeted methodologies. Furthermore, studies have indicated that pain is linked to mechanosensitive ion channels, such as PIEZO1, PIEZO2, TRPV1, and TRPV4 [36,37]. These evaluations need to be further investigated in our subsequent study. Furthermore, our research requires a more comprehensive exploration on potential mechanisms, including transcriptome changes associated with motor and sensory nerve regeneration. To fill these gaps, future studies should integrate transcriptomic analysis with behavioral assessments. This approach will provide a more detailed understanding of how blow-spun nanofibers impact cell responses and the process of nerve regeneration, particularly considering their unique fluffy structure.

In general, our study suggests that the blow-spinning technique is a promising alternative to conventional conduit fabrication methods. It is the first study to apply blow-spinning for biomaterial scaffolds fabrication, showing excellent biosafety and effectiveness. As an attractive technique for nanofiber fabrication, it can be easily translated to industry for large-scale preparation of all kinds of fibers, membranes, and 3D scaffolds for broad biomedical applications.

5. Conclusion

Blow-spinning technique and related manufacturing processing were successfully employed for collagen nanofibrous scaffolds fabrication. Based on the scalable method, a new collagen nanofibrous neuro-tube with the bilayered design was developed, incorporating inner oriented and outer random topographical cues. The bilayer structure enhances the mechanical properties of the conduit in dry and wet, displaying good radial support and suturing performance. The porous nature of the blow-spun collagen membrane enables good nutrient delivery and metabolism.

The oriented structure assumes a pivotal role in directing Schwann cells and axons, fostering myelination, and augmenting the secretion of neurotrophic factors. *In vitro* investigations have demonstrated the promising effects of bilayer conduits in expediting the myelination and growth of regenerating nerve fibers, resulting in accelerated recovery of motor function in sciatic nerve repairs. In terms of motor function recovery and extent of myelination, the new conduit approached the gold standard of autologous nerve transplantation, offering captivating prospects for translation into commercially available products. Overall, our research exemplifies an inspiring approach to the production of

nerve conduits as compelling alternatives to autologous nerve transplantation.

CRediT authorship contribution statement

Chun-Yi Yang: Conceptualization, Data curation, Formal analysis, Investigation, Methodology, Supervision, Validation, Visualization, Writing - original draft, Writing - review & editing. **Zhaohui Hou:** Conceptualization, Investigation, Methodology, Validation. **Peilun Hu:** Methodology. **Chengli Li:** Methodology. **Zifan Li:** Investigation, Methodology, Validation. **Zekun Cheng:** Formal analysis, Methodology, Data curation. **Shuhui Yang:** Data curation, Methodology, Resources. **Pengchao Ma:** Investigation, Methodology. **Zhe Meng:** Methodology. **Hui Wu:** Supervision. **Yongwei Pan:** Supervision. **Zheng Cao:** Investigation, Project administration, Supervision. **Xiumei Wang:** Conceptualization, Funding acquisition, Project administration, Supervision, Writing - review & editing.

Declaration of competing interest

A patent for the collagen nanofiber nerve guidance conduits manufacturing method (2022103271103) has been applied on behalf of Tsinghua University. X.W., Z.H., C.Y., and Z.C. are listed as inventors. The other authors declare that they have no competing interests.

Data availability

Data will be made available on request.

Acknowledgement

Y.C. and H.Z. contributed equally to this work. We acknowledge the funding support from the National Natural Science Foundation of China (No. 32271414) the Tsinghua Precision Medicine Foundation (No. 2022TS001), the Beijing Natural Science Foundation (No. L234075), and the Foshan-Tsinghua Industry-University-Research Cooperation Collaborative Innovation Project.

Appendix A. Supplementary data

Supplementary data to this article can be found online at https://doi.org/10.1016/j.mtbio.2024.100942.

References

[1] J. Scheib, A. Hoke, Advances in peripheral nerve regeneration, Nat. Rev. Neurol. 9 (12) (2013) 668–676.
[2] S.H. Yang, J.J. Zhu, C.F. Lu, Y. Chai, Z. Cao, J.J. Lu, Z. Zhang, H. Zhao, Y.Y. Huang, S.L. Yao, X.D. Kong, P.X. Zhang, X.M. Wang, Aligned fibrin/functionalized self-assembling peptide interpenetrating nanofiber hydrogel presenting multi-cues promotes peripheral nerve functional recovery, Bioact. Mater. 8 (2022) 529–544.
[3] A. Magaz, A. Faroni, J.E. Gough, A.J. Reid, X. Li, J.J. Blaker, Bioactive silk-based nerve guidance conduits for augmenting peripheral nerve repair, Adv. Healthcare Mater. 7 (23) (2018).
[4] J. Moskow, B. Ferrigno, N. Mistry, D. Jaiswal, K. Bulsara, S. Rudraiah, S. G. Kumbar, Review: bioengineering approach for the repair and regeneration of peripheral nerve, Bioact. Mater. 4 (2019) 107–113.
[5] S. Vijayavenkataraman, Nerve guide conduits for peripheral nerve injury repair: a review on design, materials and fabrication methods, Acta Biomater. 106 (2020) 54–69.
[6] C. Raza, H.A. Riaz, R. Anjum, N.U. Shakeel, Repair strategies for injured peripheral nerve: review, Life Sci. 243 (2020).
[7] V. Chiono, C. Tonda-Turo, Trends in the design of nerve guidance channels in peripheral nerve tissue engineering, Prog. Neurobiol. 131 (2015) 87–104.
[8] C.Y. Yang, W.Y. Huang, L.H. Chen, N.W. Liang, H.C. Wang, J.J. Lu, X.M. Wang, T. W. Wang, Neural tissue engineering: the influence of scaffold surface topography and extracellular matrix microenvironment, J. Mater. Chem. B 9 (3) (2021) 567–584.
[9] A. Nadaf, A. Gupta, N. Hasan, Fauziya, S. Ahmad, P. Kesharwani, F.J. Ahmad, Recent update on electrospinning and electrospun nanofibers: current trends and their applications, RSC Adv. 12 (37) (2022) 23808–23828.
[10] S.X. Chen, J.V. John, A. McCarthy, J.W. Xie, New forms of electrospun nanofiber materials for biomedical applications, J. Mater. Chem. B 8 (17) (2020) 3733–3746.
[11] J.N. Song, Z.W. Li, H. Wu, Blowspinning: a new choice for nanofibers, ACS Appl. Mater. Interfaces 12 (30) (2020) 33447–33464.
[12] Z.W. Li, Z.W. Cui, L.H. Zhao, N. Hussain, Y.Z. Zhao, C. Yang, X.Y. Jiang, L. Li, J. A. Song, B.P. Zhang, Z.K. Cheng, H. Wu, High-throughput production of kilogram-scale nanofibers by Karman vortex solution blow spinning, Sci. Adv. 8 (11) (2022).
[13] Y. Gao, J. Zhang, Y. Su, H. Wang, X.X. Wang, L.P. Huang, M. Yu, S. Ramakrishna, Y.Z. Long, Recent progress and challenges in solution blow spinning, Mater. Horiz. 8 (2) (2021) 426–446.
[14] J. Zheng, C.-Y. Yang, X. Wang, Blow-spun collagen nanofibrous spongy membrane: preparation and characterization, tissue engineering, Part C, Methods 28 (1) (2022) 3–11.
[15] Z.W. Li, J.A. Song, Y.Z. Long, C. Jia, Z.L. Liu, L. Li, C. Yang, J.C. Liu, S. Lin, H. Y. Wang, Y.B. Liu, M.H. Fang, H. Wu, Large-scale blow spinning of heat-resistant nanofibrous air filters, Nano Res. 13 (3) (2020) 861–867.
[16] W.-H. Huang, S.-L. Ding, X.-Y. Zhao, K. Li, H.-T. Guo, M.-Z. Zhang, Q. Gu, Collagen for neural tissue engineering: materials, strategies, and challenges, Materials Today Bio 20 (2023) 100639.
[17] C.Y. Wang, T. Yokota, T. Someya, Natural biopolymer-based biocompatible conductors for stretchable bioelectronics, Chem. Rev. 121 (4) (2021) 2109–2146.
[18] K.L. Lin, D.W. Zhang, M.H. Macedo, W.G. Cui, B. Sarmento, G.F. Shen, Advanced collagen-based biomaterials for regenerative biomedicine, Adv. Funct. Mater. 29 (3) (2019).
[19] B.J. Parker, D.I. Rhodes, C.M. O'Brien, A.E. Rodda, N.R. Cameron, Nerve guidance conduit development for primary treatment of peripheral nerve transection injuries: a commercial perspective, Acta Biomater. 135 (2021) 77–99.
[20] X. Zhang, W.R. Qu, D. Li, K. Shi, R. Li, Y.Q. Han, E. Jin, J.X. Ding, X.S. Chen, Functional polymer-based nerve guide conduits to promote peripheral nerve regeneration, Adv. Mater. Interfac. 7 (14) (2020).
[21] S.Y. Wang, F. Yan, P. Ren, Y. Li, Q. Wu, X.D. Fang, F.F. Chen, C. Wang, Incorporation of metal-organic frameworks into electrospun chitosan/poly (vinyl alcohol) nanofibrous membrane with enhanced antibacterial activity for wound dressing application, Int. J. Biol. Macromol. 158 (2020) 9–17.
[22] V.Y. Chakrapani, A. Gnanamani, V.R. Giridev, M. Madhusoothanan, G. Sekaran, Electrospinning of type I collagen and PCL nanofibers using acetic acid, J. Appl. Polym. Sci. 125 (4) (2012) 3221–3227.
[23] J.R. Du, J.H. Liu, S.L. Yao, H.Q. Mao, J. Peng, X. Sun, Z. Cao, Y.D. Yang, B. Xiao, Y. G. Wang, P.F. Tang, X.M. Wang, Prompt peripheral nerve regeneration induced by a hierarchically aligned fibrin nanofiber hydrogel, Acta Biomater. 55 (2017) 296–309.
[24] S. Ryglova, M. Braun, T. Suchy, Collagen and its modifications-crucial aspects with concern to its processing and analysis, Macromol. Mater. Eng. 302 (6) (2017).
[25] S.H. Yang, C. Wang, J.J. Zhu, C.F. Lu, H.T. Li, F.Y. Chen, J.J. Lu, Z. Zhang, X. Q. Yan, H. Zhao, X.D. Sun, L.Y. Zhao, J. Liang, Y. Wang, J. Peng, X.M. Wang, Self-assembling peptide hydrogels functionalized with LN- and BDNF- mimicking epitopes synergistically enhance peripheral nerve regeneration, Theranostics 10 (18) (2020) 8227–8249.
[26] N. Stikov, J.S.W. Campbell, T. Stroh, M. Lavelee, S. Frey, J. Novek, S. Nuara, M. K. Ho, B.J. Bedell, R.F. Dougherty, I.R. Leppert, M. Boudreau, S. Narayanan, T. Duval, J. Cohen-Adad, P.A. Picard, A. Gasecka, D. Cote, G.B. Pike, In vivo histology of the myelin g-ratio with magnetic resonance imaging, Neuroimage 118 (2015) 397–405.
[27] S. Yi, L. Xu, X.S. Gu, Scaffolds for peripheral nerve repair and reconstruction, Exp. Neurol. 319 (2019).
[28] Y. Qian, H. Lin, Z.W. Yan, J.L. Shi, C.Y. Fan, Functional nanomaterials in peripheral nerve regeneration: scaffold design, chemical principles and microenvironmental remodeling, Mater. Today 51 (2021) 165–187.
[29] J.L. Daristotle, A.M. Behrens, A.D. Sandler, P. Kofinas, A review of the fundamental principles and applications of solution blow spinning, ACS Appl. Mater. Interfaces 8 (51) (2016) 34951–34963.
[30] X. Dong, S. Liu, Y. Yang, S. Gao, W. Li, J. Cao, Y. Wan, Z. Huang, G. Fan, Q. Chen, H. Wang, M. Zhu, D. Kong, Aligned microfiber-induced macrophage polarization to guide schwann-cell-enabled peripheral nerve regeneration, Biomaterials 272 (2021) 120767.
[31] S. Houshyar, A. Bhattacharyya, R. Shanks, Peripheral nerve conduit: materials and structures, ACS Chem. Neurosci. 10 (8) (2019) 3349–3365.
[32] Y. Yan, R. Yao, J. Zhao, K. Chen, L. Duan, T. Wang, S. Zhang, J. Guan, Z. Zheng, X. Wang, Z. Liu, Y. Li, G. Li, Implantable nerve guidance conduits: material combinations, multi-functional strategies and advanced engineering innovations, Bioact. Mater. 11 (2022) 57–76.
[33] W. Zhou, M.S.U. Rahman, C. Sun, S. Li, N. Zhang, H. Chen, C.C. Han, S. Xu, Y. Liu, Perspectives on the Novel Multifunctional Nerve Guidance Conduits: from Specific Regenerative Procedures to Motor Function Rebuilding, Advanced Materials, Deerfield Beach, Fla., 2023 e2307805.
[34] Y. Kong, W. Shi, D. Zhang, X. Jiang, M. Kuss, B. Liu, Y. Li, B. Duan, Injectable, antioxidative, and neurotrophic factor-deliverable hydrogel for peripheral nerve regeneration and neuropathic pain relief, Appl. Mater. Today 24 (2021) 101090.
[35] F. Liang, Y. Yang, Y. Chen, J. Xie, S. Liu, Z. Tan, L. Tian, Z. Yu, Z. Shi, P. Xie, H. Ding, Q. Yang, Ropivacaine microsphere-loaded electroconductive nerve

dressings for long-acting analgesia and functional recovery following diabetic peripheral nerve injury, Materials Today Bio 21 (2023) 100712.
[36] J. Acheta, U. Bhatia, J. Haley, J.Y. Hong, K. Rich, R. Close, M.E. Bechler, S. Belin, Y. Poitelon, Piezo channels contribute to the regulation of myelination in Schwann cells, Glia 70 (12) (2022) 2276–2289.
[37] N.W. Villarino, Y.M.F. Hamed, B. Ghosh, A.E. Dubin, A.H. Lewis, M.A. Odem, M. C. Loud, Y. Wang, M.R. Servin-Vences, A. Patapoutian, K.L. Marshall, Labeling PIEZO2 activity in the peripheral nervous system, Neuron 111 (16) (2023) 2488–2501.e8.